JOURNAL OF PROPULSION AND POWER
Vol. 14, No. 6, November–December 1998

Potential Field Interactions in a Low-Speed Centrifugal Compressor

Albert J. Sanders* and Sanford Fleeter†
Purdue University, West Lafayette, Indiana 47907

A series of experiments is performed to investigate the unsteady aerodynamic response of a centrifugal compressor impeller resulting from its interaction with the potential field of the downstream radial-vaned diffuser. Fundamental unsteady impeller–diffuser aerodynamic interaction data are acquired at two impeller–diffuser radial spacings over a wide range of flow rates. The detailed diffuser vane-generated unsteady aerodynamic forcing function and the resulting impeller-blade unsteady aerodynamic response are measured and analyzed. Very near the diffuser-vane leading-edge plane, multiple harmonics are required to describe the spatially nonuniform static pressure field generated by the diffuser vanes. However, the higher harmonic components associated with this potential flow-generated forcing-function decay very rapidly across the vaneless space, and the impeller blades respond primarily to the first harmonic. The maximum impeller-blade unsteady aerodynamic loading also occurs near the midchord region, and not near the exit where the diffuser vane generated forcing function is largest. Increasing the radial spacing between the impeller and diffuser significantly reduces both the amplitude of the forcing function and resulting impeller-blade unsteady aerodynamic loading.

Nomenclature

A_e = impeller exit area
C_p = unsteady pressure coefficient describing impeller-blade response
$\bar{C}_p$ = steady pressure coefficient, $(p - p_\infty)/1/2\rho_\infty U_w^2$
C_p' = fluctuating static pressure coefficient describing forcing function
i = mass-averaged incidence angle, positive counterclockwise
P_t = total pressure
p = static pressure
$\bar{p}$ = unsteady first harmonic surface pressure
p_{av} = average static pressure across a full vane passage
p_∞ = ambient pressure
Q = volume flow rate
R = diffuser vane leading edge to impeller exit radius ratio
R^* = hot-film traverse to impeller exit radius ratio
U_w = wheel speed at mean impeller exit radius
V = absolute velocity magnitude
ρ_∞ = ambient density
ϕ = flow coefficient, $Q/A_e U_w$
ψ = pressure rise coefficient, $(P_{t,\mathrm{dn}} - P_{t,\mathrm{up}})/1/2\rho_\infty U_w^2$

Introduction

IMPELLER-BLADE resonant-forced vibration is an area of important concern in the design and development of advanced centrifugal compressors. These vibrations occur when a periodic forcing function, with a frequency at or near an impeller-blade's natural frequency, acts on the impeller. The primary forcing function to the impeller is the potential field of the downstream radial-vaned diffuser, i.e., the steady spatially nonuniform potential flowfield of the diffuser vanes acts as a temporal excitation to the rotating impeller (Fig. 1).

Campbell diagrams are commonly used to analyze the forced-response behavior of a centrifugal compressor design. However, the amplitudes of the resonant stresses on the impeller blades cannot be predicted because the Campbell diagrams do not consider the details of the unsteady aerodynamic forcing function or the resultant impeller-blade unsteady aerodynamics. Thus, the stress amplitudes are not known until first build rig testing of the component. If excessive stresses are encountered, costly redesigns are necessary to alter the critical intersection point on the Campbell diagram, thereby alleviating the problem. This is accomplished by either redesigning the impeller to change its natural frequencies and/or changing the diffuser geometry, thereby changing the magnitude and frequency of the unsteady aerodynamic forcing function. Unfortunately, there are limited radial-flow tubomachine mathematical models to access the overall effects of these changes, with a trial and error approach typically utilized to reduce the stresses to acceptable levels.

Considering the frequency of occurrence of these forced-response problems, it is surprising that so little research has focused on addressing the unsteady aerodynamics of radial-flow turbomachine blade rows. Inoue and Cumpsty[1] experimentally investigated the unsteady impeller–diffuser interaction in a low-speed centrifugal compressor with radial spacings ranging from 4 to 20% of the impeller exit radius. The static pressure rise characteristics through the impeller were up to 6% larger for vaned configurations as compared to vaneless builds caused by enhanced mixing of the jet and wake inside the impeller channel. Arndt et al.[2] performed an experimental study of the diffuser vane response caused by blade row interactions in a high-performance turbopump with the impeller–diffuser radial spacing ranging from 1.5 to 4.5% of the impeller exit radius. The amplitude of the ensemble-averaged lift was found to be up to three times larger than the steady lift for a radial spacing of 1.5% and up to two times larger for a radial spacing of 4.5%. In a later study they analyzed the impeller-blade and diffuser-vane responses for several vaned-diffuser configurations with radial spacings ranging from 5 to 8% of the impeller exit radius.[3] For small radial spacings the pressure fluctuations on the impeller blades and diffuser vanes could be the same order of magnitude as the total pressure rise across the pump.

Received April 15, 1997; revision received Dec. 1, 1997; accepted for publication March 10, 1998.

*Research Assistant, School of Mechanical Engineering, 1003 Chaffee Hall. Student Member AIAA.

†McAllister Distinguished Professor, School of Mechanical Engineering, 1003 Chafee Hall. Associate Fellow AIAA.

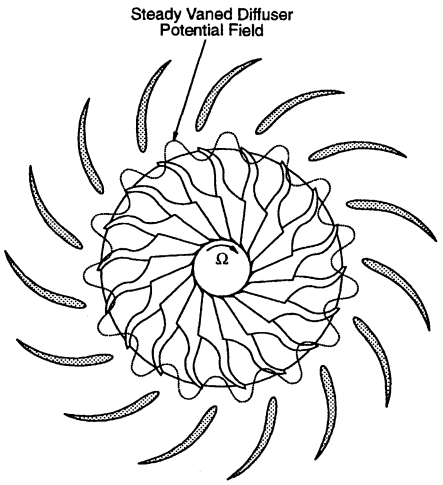

Fig. 1 Unsteady aerodynamic forcing function to a centrifugal compressor impeller.

Fisher and Inoue[4] developed a theoretical model that combined a conformal transformation with the steady Martensen surface singularity theory to predict the induced velocity field of the diffuser at the impeller exit. Comparing theoretical predictions with low-speed centrifugal compressor data, they reported good agreement for cases when the diffuser flow was not separated. Their model enabled the designer to specify the radial spacing between the impeller and diffuser necessary to modulate the induced velocity perturbations to an acceptable level. Bryan and Fleeter[5] developed a model to predict the unsteady aerodynamic loading of a radial airfoil cascade caused by pitching and plunging airfoil motions as well as a convected vortical gust. Their analysis is based on conformally mapping a solution obtained from the incompressible flat-plate cascade model of Whitehead[6] to a radial cascade consisting of logarithmic spiral airfoils.

Caruthers and Kurosaka[7] developed a small perturbation analysis of a one-dimensional steady flow to predict the distribution of the unsteady aerodynamic loading on impeller blades generated by a vaned-diffuser potential field. The one-dimensional steady flow has a constant Mach number through the impeller-blade passage, thereby capturing some features of the jet-wake effect found in actual impellers, i.e., the jet in the impeller passage has been found experimentally to have a nearly constant Mach number. However, one-dimensional steady flow through a rotating impeller is not consistent with the small perturbation velocity potential equation that requires the steady flow to be irrotational.

In summary, little research has been directed at the unsteady aerodynamics and forced-response characteristics of radial-flow turbomachines. Thus, relatively little is known about the unsteady impeller–diffuser interactions that occur within centrifugal compressors. Because these unsteady aerodynamic interactions can lead to high vibratory stresses in both the impeller blades and diffuser vanes, mathematical models must be developed to analyze radial-flow turbomachine blade rows. In addition, relevant experiments are needed to assess the validity of these math models and to direct future research efforts.

The objective of this research is to investigate and quantify the fundamental impeller–diffuser interaction phenomena relevant to impeller-blade forced vibration driven by the potential field of the downstream radial vaned diffuser. This is accomplished by performing a series of experiments in the Purdue Low-Speed Centrifugal Compressor, a highly flexible large-scale facility that features a shrouded mixed-flow impeller and a radial-vaned diffuser. The forcing function to the impeller blades is the potential field generated by the downstream-vaned diffuser. Both this unsteady aerodynamic forcing function and the resultant impeller blade unsteady aerodynamic response are experimentally measured. In particular, the radial spacing between the impeller exit and the diffuser vane inlet is varied, with the resulting impeller–diffuser unsteady aerodynamic interactions measured and analyzed.

Research Facility

The Purdue Low-Speed Centrifugal Compressor is a large-scale facility that features a shrouded mixed-flow impeller followed by a radial-vaned diffuser. The compressor is belt driven by a 29.8-kW (40-hp) induction motor that rotates the impeller at 1790 rpm. A cutaway view of the facility is shown in Fig. 2.

The impeller has an average exit diameter of 73.2 cm (28.8 in.) and consists of 23 backswept blades cast integrally with the hub, with the backsweep angle at the impeller exit 51 deg. The blade design is of a deloaded type in which the pressure surface is concave over the first part of the passage and convex over the remainder. This reversal of curvature tends to reduce the aerodynamic loading near the blade exit while increasing the loading over the central portion of the blade.

The diffuser consists of a curved vaneless space that smoothly turns the flow into the radial direction followed by a parallel-wall, radial-vaned diffuser. The cambered diffuser vanes have a NACA 4312 airfoil profile with a chord length of 16.5 cm (6.5 in.). The vanes are mounted on eccentric cams embedded in the diffuser endwall. This mounting arrangement allows both the stagger angle and the vane leading-edge radius to be varied independently. In addition, the vanes are removable so that the facility can be configured with a maximum of 30 vanes, a reduced set of either 15 or 10 vanes, or in a vaneless configuration. For this series of experiments, the diffuser is configured with 15 vanes set at a stagger angle of 60 deg.

Data Acquisition and Analysis

The data of fundamental interest include the detailed unsteady aerodynamic forcing function to the rotating impeller and the resulting impeller blade unsteady aerodynamic response. Measurements of the compressor performance are also needed to define the compressor operating conditions at which these detailed unsteady aerodynamic data are acquired.

Potential Field Forcing-Function Analysis

The periodic forcing function to the impeller is the steady circumferentially nonuniform static pressure variation generated by the downsteam diffuser vane potential field. This static pressure variation is determined from time-averaged midspan measurements of both the velocity field and the total pressure

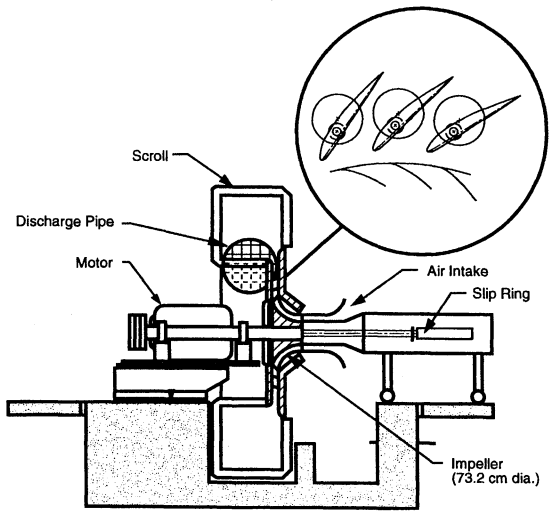

Fig. 2 Purdue Low-Speed Centrifugal Compressor Research Facility.

at the diffuser inlet, with the survey radius for these measurements 39.5 cm (15.55 in.). The velocity measurements are made by traversing a slanted, single-sensor hot-film anemometer probe across one complete diffuser vane passage. The circumferential survey points are equally spaced with 1 deg intervals, yielding a total of 25 points across the vane passage. In addition, the total pressure is measured at midpassage using a pneumatic total pressure probe. The static pressure variation across the vane passage is then calculated from the Bernoulli equation.

$$p = P_t - 1/2\rho_\infty V^2 \tag{1}$$

where P_t is the total pressure at midpassage, and V is the velocity magnitude at each survey point.

The forcing function is then defined by the following fluctuating static pressure coefficient, with a Fourier analysis enabling this forcing function to be described in terms of its spatial harmonics. The impeller blade response to each harmonic of this forcing function may then be analyzed:

$$C_p' = \frac{p - p_{av}}{1/2\rho_\infty U_w^2} \tag{2}$$

The estimated uncertainty in this coefficient is 3.5%.

A slanted single-sensor hot-film anemometer is used to measure the time-average three-dimensional velocity field at the diffuser inlet. A TSI Corporation hot-film anemometer is employed and consists of an IFA 100 Intelligent Flow Analyzer and a model 1213-20 slanted, single-sensor platinum hot-film probe. The sensor is slanted 45 deg from the axis of the probe with an active sensing length of 1.0 mm and a sensor diameter of 51 μm. The three components of the velocity are resolved by acquiring data at each of three angular settings of the probe, with the data reduced using a second-order empirical correlation for the sensor response.[8] From the calibration it was determined that probe yaw-angle combinations of +50, +20, and −10 or +50, +20, and −40 deg yielded the lowest errors over the range of velocities an pitch angles encountered in the facility. Thus at each survey point, the probe was rotated until the sensor was approximately aligned with the mean flow direction, characteristically given by a minimum anemometer output voltage signal. The probe was then rotated +50, +20, −10, and −40 deg relative to this point and the resultant output voltage recorded, with the voltages corresponding to probe orientation combinations of +50, +20, and −10 or +50, +20, and −40 deg used to reduce the data.

Impeller Blade Unsteady Loading Analysis

The unsteady midspan surface pressure distribution on the impeller blades is measured by instrumenting the pressure surface of one blade and the suction surface of an adjacent blade with PCB 103A miniature microphone pressure transducers. The transducers have a nominal sensitivity of 0.22 mV/Pa (1500 mV/psi) and a natural frequency of 13 kHz. The locations of these transducers are tabulated in Table 1 and shown schematically in Fig. 3. To account for possible signal attenuation and/or phase shift because of installation and mounting, the transducers are dynamically calibrated after installation and prior to each run. The periodic component of the microphone signal is recovered using a digital ensemble-averaging technique. A fast Fourier transform is then performed on these conditioned signals to determine the harmonic content.

The unsteady impeller-blade loading distribution is described by an unsteady surface pressure coefficient

$$C_p = \bar{p}/1/2\rho_\infty U_w^2 \tag{3}$$

The estimated uncertainties in the magnitude and phase angle of this coefficient are 0.25% and 0.1 deg, respectively.

Table 1 Impeller-blade unsteady pressure-transducer locations

Pressure surface		Suction surface	
Percent meridional chord	Radial location, r/r_0	Percent meridional chord	Radial location, r/r_0
4.87	0.560	2.1	0.555
14.5	0.562	11.2	0.559
36.8	0.620	34.8[a]	0.620[a]
58.2	0.719	55.8	0.714
74.2	0.811	72.0	0.802
83.1	0.874	79.8	0.854
89.3	0.917	86.8	0.906
95.0	0.963	93.2	0.954

[a]Inoperative transducer.

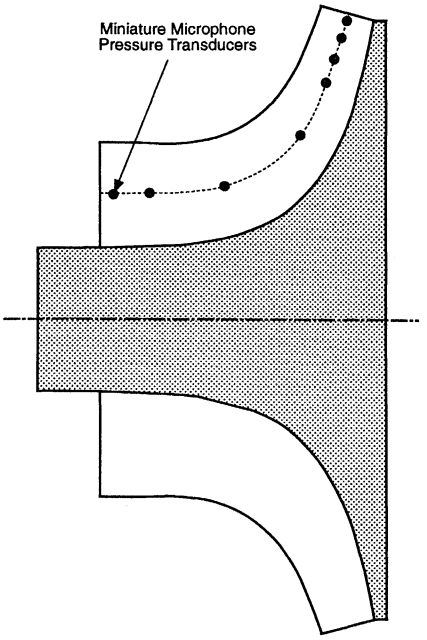

Fig. 3 Meridional view of impeller-blade unsteady pressure transducer locations.

Computer-Controlled Data-Acquisition System

The data-acquisition system is controlled using an Apple Macintosh Quadra 950 personal computer and an HP3497A Data Acquisition and Control Unit. The instantaneous time-variant signals are acquired and digitized using a National Instruments NB-A2000 A/D conversion board.

To measure the steady spatially nonuniform velocity field at the diffuser inlet, the signal from the hot-film anemometer probe is digitized at a rate of 75 kHz, with the number of samples chosen to encompass 100 complete impeller revolutions. These digitized signals are then arithmetically averaged to obtain the time-mean voltage. The sampling rate and number of samples is chosen to be sufficiently high so that both random and periodic unsteadiness are averaged out.

The time-variant signals from the instrumented impeller blades are transferred to the stationary reference frame using a 46-channel wetted mercury slip ring, where they are amplified and then remotely multiplexed. The multiplexed voltages are then digitized at a rate of 50 kHz and ensemble-averaged over 500 impeller revolutions, with the number of samples chosen to correspond to one full impeller revolution. The resultant frequency resolution is 29.83 Hz, which corresponds to a once-per-revolution disturbance.

Results

A series of experiments is performed in the Purdue Low-Speed Centrifugal Compressor Facility to investigate the un-

steady impeller blade response because of its interaction with the potential field of the downstream radial vaned diffuser. Detailed measurements of both the unsteady aerodynamic forcing function and the resultant impeller blade unsteady surface pressure distributions are made at flow coefficients of 0.30, 0.22, and 0.17 for each of two different diffuser vane leading edge to impeller exit radius ratios, R = 1.10 and R = 1.15. These operating points are shown on the compressor characteristic in Fig. 4.

Figure 5 shows the midspan impeller blade and diffuser vane steady loading distributions for the small radial spacing as a function of meridional chord for each of these operating points. Details regarding the tap locations and measurement procedures can be found in Bryan.[9] The loading distributions for the large radial spacing are very similar and are thus not presented. The impeller loading is very uniform across the entire chord, whereas the diffuser vane loading is highest in the leading-edge region. High levels of steady loading also occur near the impeller trailing edge, which is attributed the constant thickness blades having round leading and trailing edges. Additionally, there is no evidence of flow separation on either the

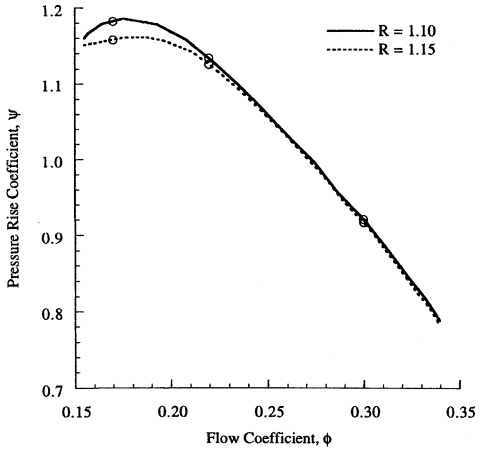

Fig. 4 Operating points at which data were acquired.

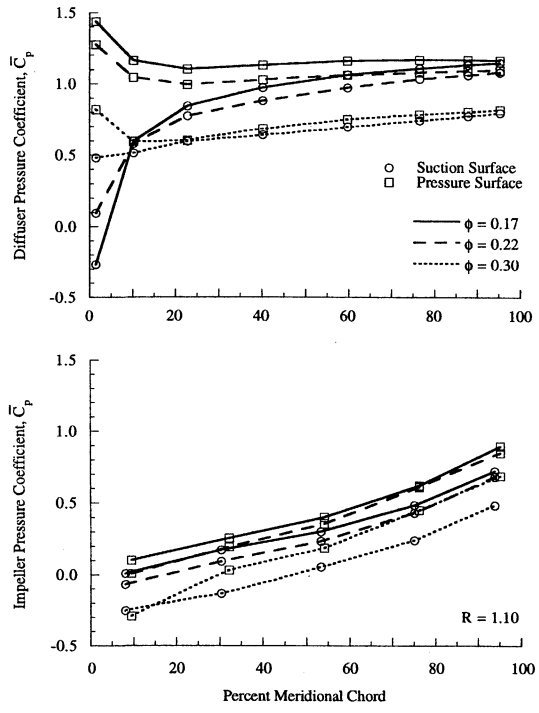

Fig. 5 Impeller and diffuser steady loading distributions for small radial spacing.

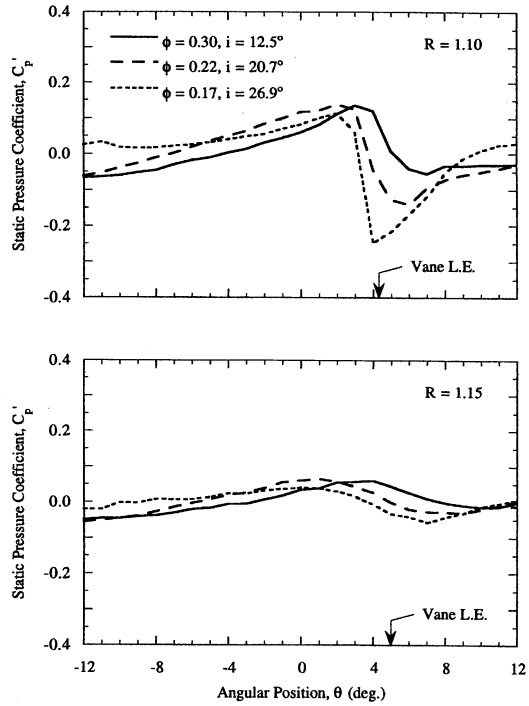

Fig. 6 Effect of steady loading on forcing-function waveform.

impeller blades or diffuser vanes for all operating points investigated. However, the diffuser vane pressure distributions are beginning to flatten out at the lower flow rates, indicating that the diffuser may be setting the machine performance.

The forcing function to the impeller is the time-average spatially nonuniform static pressure field generated by the diffuser vanes. Figure 6 shows this static pressure field at the diffuser inlet for both impeller–diffuser radial spacings as a function of the compressor loading or flow coefficient. As the flow coefficient is reduced from 0.30 to 0.17, the mass-averaged incidence angle to the diffuser vanes increases from 12.5 to 26.9 deg for the small spacing, and from 13.4 to 30.8 deg for the large spacing, thereby increasing the diffuser vane steady loading. Note that the measurements of the forcing function for both impeller–diffuser radial spacings are made at the same radius ratio, R^* = 1.079. Changing the radial spacing, however, increases the distance between the diffuser inlet where the measurements were made and the vane leading-edge plane. Thus, the results for the larger spacing show the decay of the forcing function with radius.

The static pressure fluctuations reach quite large amplitudes near the vane leading edge for the small spacing, ranging from ±10% of the dynamic pressure based on the wheel speed at the lowest loading to ±18% at the highest. For the larger spacing, the fluctuations are considerably reduced, being around ±5% for all three loading levels. The phase angle of the waveforms for both radial spacings also changes with steady loading, with the peaks corresponding to the minimum and maximum amplitudes moving to the left as the loading is increased.

The static pressure forcing function waveforms are Fourier decomposed into harmonics for both radial spacings at low-, moderate-, and high-loading levels. With the diffuser vanes lightly loaded, the waveform of the forcing function for both radial spacings is primarily composed of the first harmonic (Fig. 7), with the higher harmonics being much smaller. Note that the first harmonic amplitude is quite large, being 7 and 4.5% of the dynamic pressure based on the wheel speed for the small and large impeller–diffuser radial spacings, respectively.

Figure 8 shows the results of the forcing-function Fourier analysis for moderate vane loading. Increasing the steady loading, and thus the incidence to the vane row, causes all of the

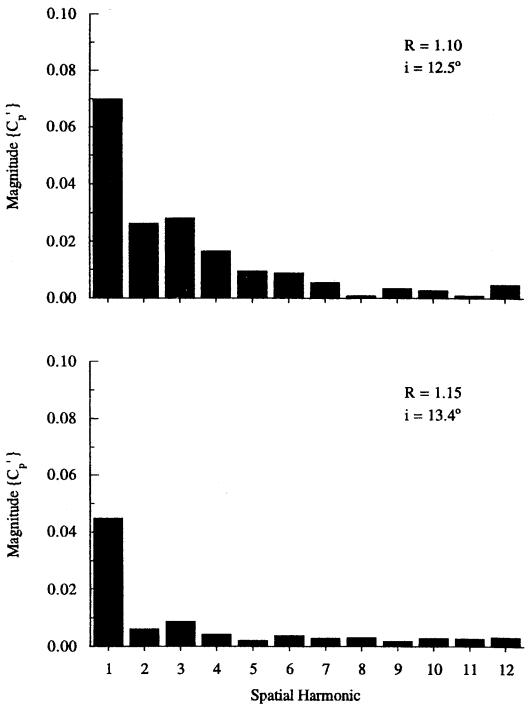

Fig. 7 Fourier analysis of forcing function for low-steady loading (ϕ = 0.30).

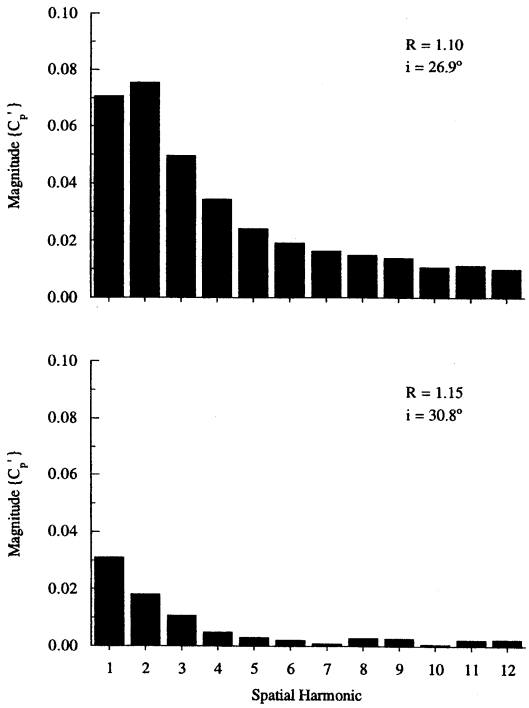

Fig. 9 Fourier analysis of forcing function for high-steady loading (ϕ = 0.17).

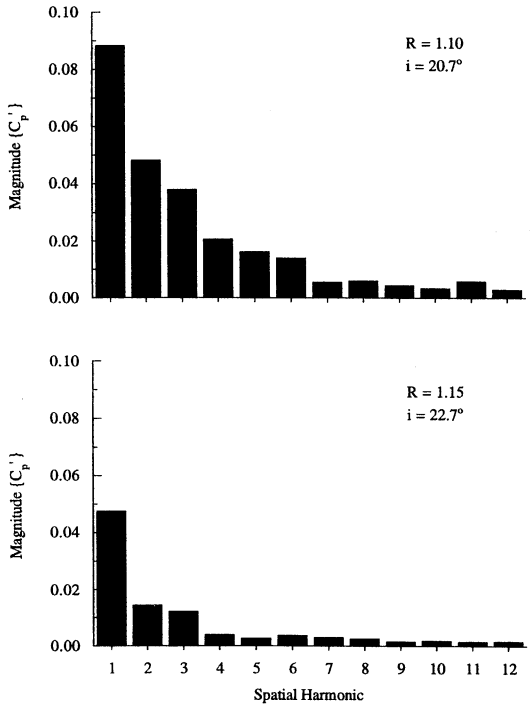

Fig. 8 Fourier analysis of forcing function for moderate-steady loading (ϕ = 0.22).

harmonic amplitudes to increase. For the small radial spacing, the first three harmonics of the forcing function are significant, ranging from 4 to 9% of the dynamic pressure. At the larger spacing the forcing function is still composed primarily of the first harmonic alone, with this amplitude being nearly 5% of the dynamic pressure.

Figure 9 shows the harmonic decomposition of the forcing function corresponding to the highest vane loading. It is surprising that the first harmonic amplitudes have decreased relative to their values at the two lower loading conditions, with this trend present for both radial spacings. However, the increased vane loading results in the higher harmonics of the forcing function increasing in amplitude. In fact, at the small spacing, the amplitude of the second harmonic is actually larger than that of the first, with the first four harmonics being of significant amplitude. For the large spacing, even though the second and third harmonic amplitudes have increased, they still remain quite small. Thus, for small impeller–diffuser radial spacings, multiple spatial harmonics are required to describe the detailed forcing function to the impeller blades.

The spatially nonuniform vaned diffuser potential flowfield acts as a temporal excitation to the rotating impeller. As multiple harmonics have been found to be required to describe this diffuser vane-generated static pressure field for the small impeller–diffuser radial spacing, it is first necessary to determine the harmonics of the forcing function to which the impeller blades respond. This is accomplished by examining the harmonic content of the pressure fluctuations near the impeller-blade trailing edge.

Figures 10–12 show the magnitude of the unsteady pressure coefficients determined from the pressure and suction surface transducers nearest the trailing edge for frequencies up to five times vane pass. The impeller-blade response is primarily composed of the first harmonic of vane-pass frequency, with the magnitudes of the higher harmonics negligible. As the flow coefficient is reduced, thereby increasing the steady loading, the amplitudes of these first harmonic pressure fluctuations on both blade surfaces increase significantly for both radial spacings, by nearly a factor of 2 as the flow coefficient is reduced from 0.30 to 0.17. At the large spacing, the amplitudes of the pressure fluctuations are reduced by nearly 50% over those occurring at the small spacing for all operating points. The once per revolution disturbance is attributed to the exit distortion caused by the scroll outlet, with the resultant impeller-blade response independent of the impeller–diffuser spacing at each operating point.

Although multiple harmonics are required to describe the diffuser inlet spatially nonuniform static pressure field, the higher harmonics decay very rapidly across the vaneless space and the impeller blades respond primarily to the first harmonic

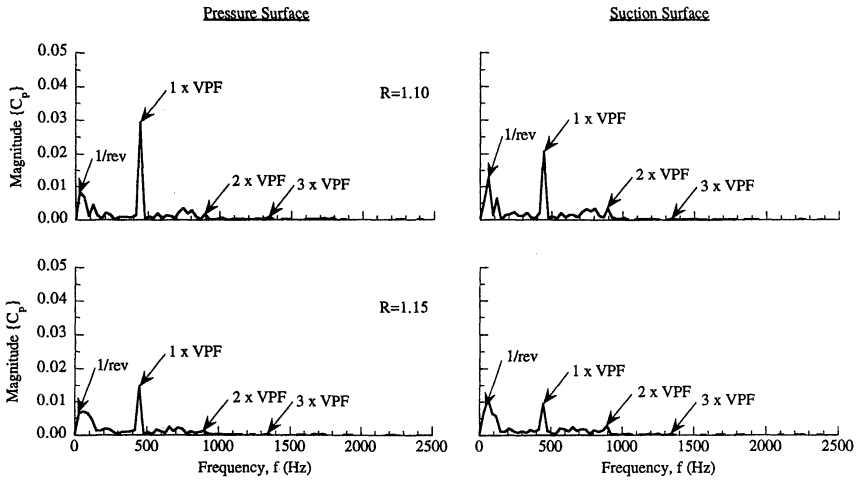

Fig. 10 Impeller-blade trailing-edge spectrum for low-steady loading (ϕ = 0.30).

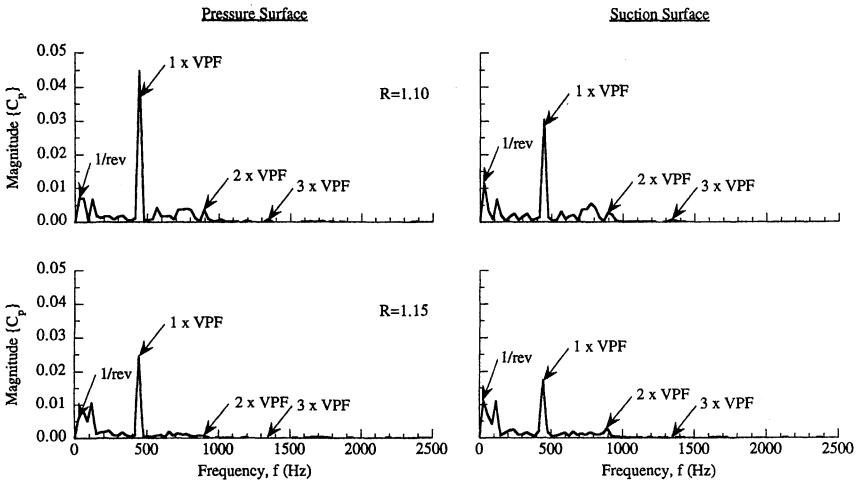

Fig. 11 Impeller-blade trailing-edge spectrum for moderate-steady loading (ϕ = 0.22).

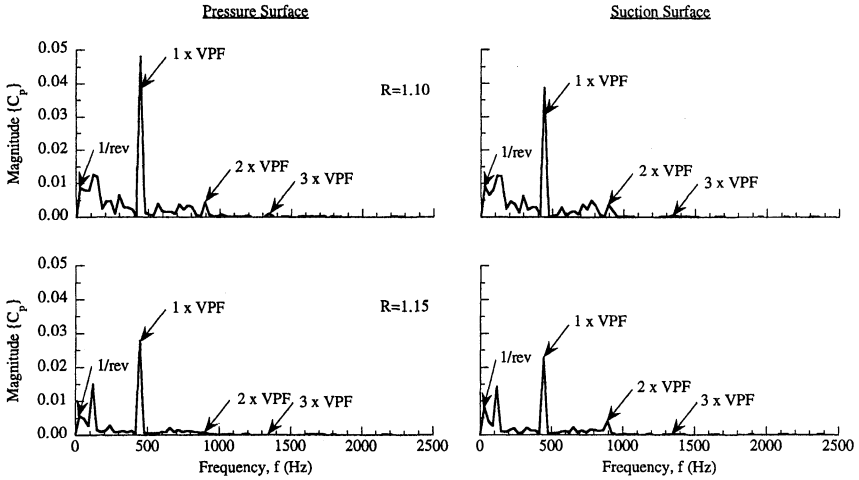

Fig. 12 Impeller-blade trailing-edge spectrum for high-steady loading (ϕ = 0.17).

of this forcing function. Thus, for the subsequent analysis, only the first harmonic impeller-blade surface pressure distributions are considered. In particular, both the unsteady pressure difference across the blade and the individual pressure and suction surface loading distributions are analyzed (Figs. 13–18). These complex pressure distributions are presented in terms of a magnitude and a phase angle as a function of the steady compressor loading, with the blade surface pressures nondimensionalized by the dynamic pressure based on the impeller wheel speed at the mean exit radius, and the phase angles referenced to the data initiation pulse.

Figures 13 and 14 show the unsteady pressure distribution along the impeller-blade pressure surface as a function of the compressor loading for the small and large impeller–diffuser radial spacings. The maximum amplitudes of the pressure distributions occur near 40% chord for both radial spacings. Because the amplitude of the forcing function is highest at the impeller exit, it was expected that the surface pressure fluc-

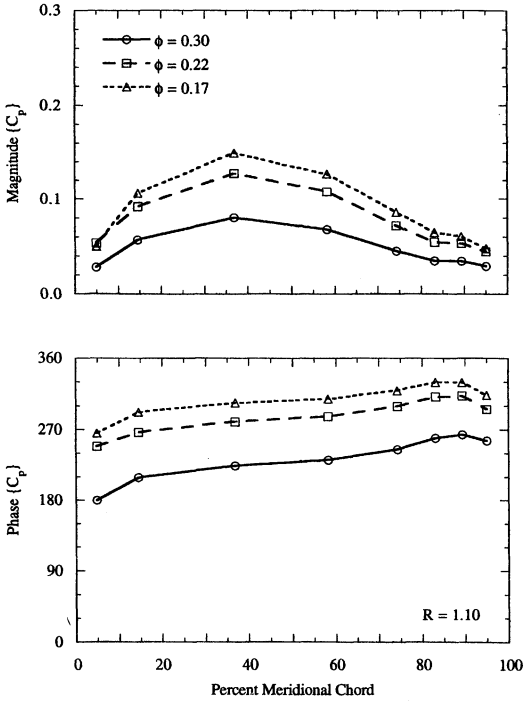

Fig. 13 Effect of steady loading on pressure surface unsteady pressure for small spacing.

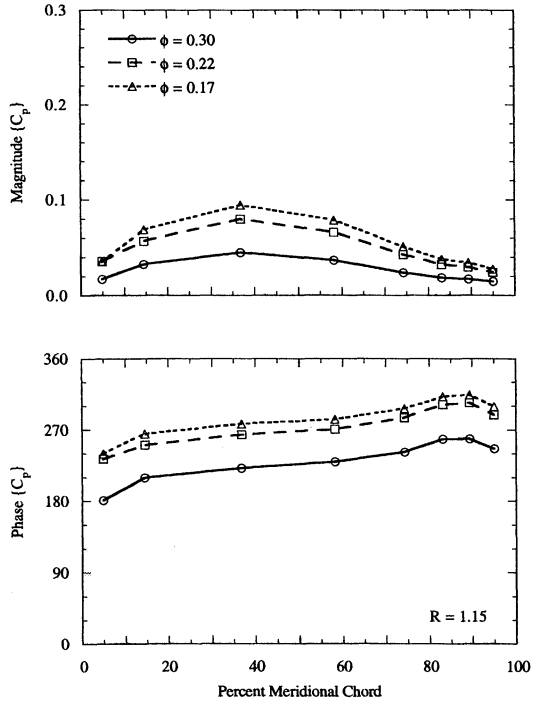

Fig. 14 Effect of steady loading on pressure surface unsteady pressure for large radial spacing.

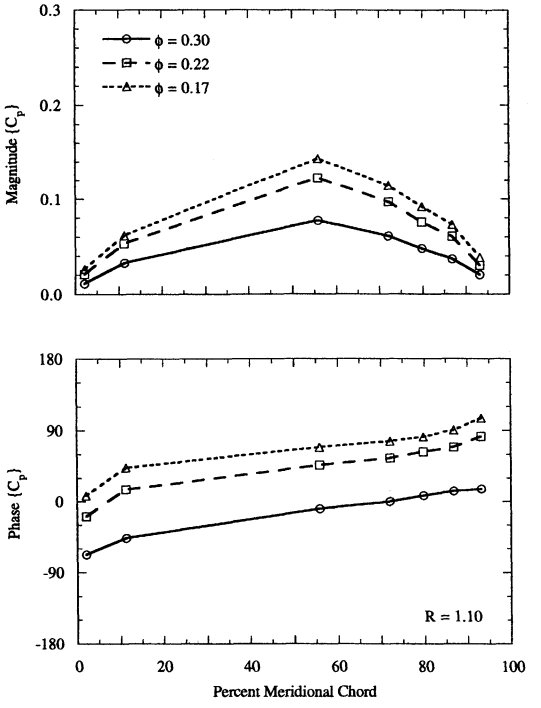

Fig. 15 Effect of steady loading on suction surface unsteady pressure for small radial spacing.

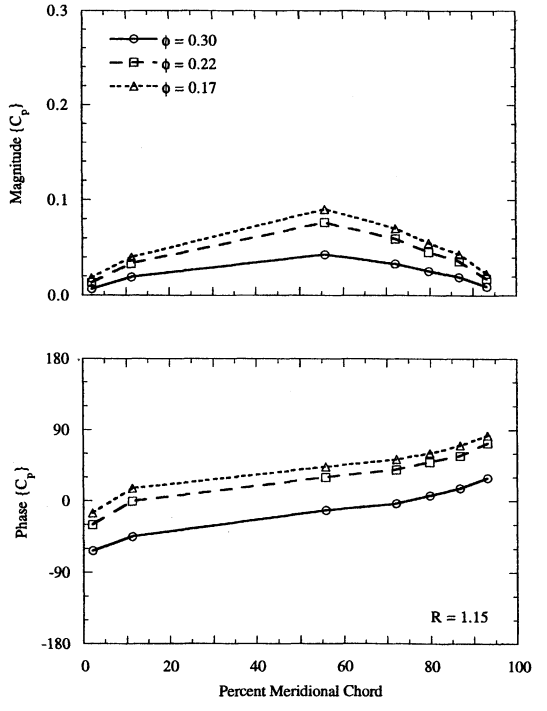

Fig. 16 Effect of steady loading on suction surface unsteady pressure for large radial spacing.

tuations would also be highest in this region. The data, however, reveal that the entire pressure surface of the blade responds as a result of the interaction, with the unsteady pressure fluctuations highest over the middle portion of the blade. Perhaps this is a result of the blade-to-blade spacing in the impeller-inducer section being much smaller than that at the exit. The close proximity of the neighboring blades in this region may give rise to an increased interaction, or cascading effect, which would be unique to centrifugal turbomachines. Additionally, the pressure distributions remain fairly flat over the aft 20% of the blade, with increased steady loading resulting in an increased pressure-fluctuation amplitude.

The phase angles follow a nearly linear trend between 20 and 80% chord, increasing as one moves aft along the blade. This linear increase implies that a disturbance originating downstream propagates upstream along the blade chord, which may be a result of acoustic interactions between the impeller and diffuser. Also, the phase angle at any given chordwise location increases as the loading is increased, i.e., as the flow coefficient is reduced. This trend is also apparent in the forc-

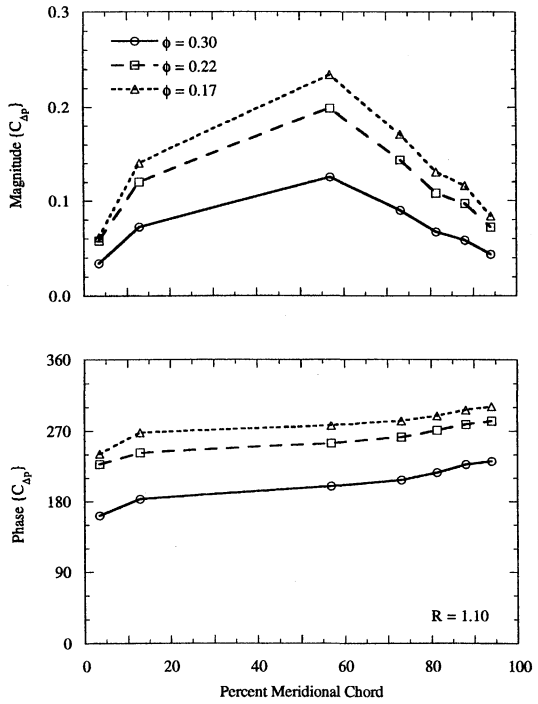

Fig. 17 Effect of steady loading on unsteady pressure difference for small radial spacing.

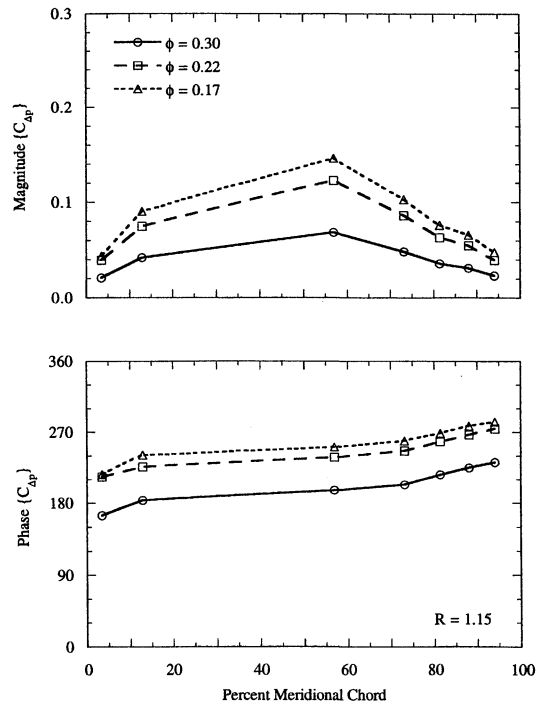

Fig. 18 Effect of steady loading on unsteady pressure difference for large radial spacing.

ing-function waveforms, with the phase angles of the static pressure perturbations increasing as the steady loading increases, i.e., the waveforms shift to the left.

The suction-surface pressure distributions shown in Figs. 15 and 16 follow an analogous trend as those noted for the pressure surface. For both radial spacings, the pressure fluctuations are highest just aft of midchord, whereas for the pressure surface they were highest just forward of this location. Increasing the steady compressor loading results in an increase in the amplitude of these suction surface pressure fluctuations. Additionally, the unsteady pressures on the suction surface lag those on the pressure surface by a nearly constant value of 90 deg over most of the blade for all three steady loading levels. However, near the trailing edge, the unsteady pressure on the suction surface is nearly 180 deg out of phase with that on the pressure surface.

The unsteady pressure difference across the impeller blade for the small and large radial spacings is shown in Figs. 17 and 18, with the pressure difference defined as pressure surface minus suction surface. The unsteady loading increases as the steady loading level is increased for both radial spacings. This trend is surprising because the first harmonic amplitude of the forcing function reached a maximum at a flow coefficient of 0.22 and decreased thereafter. One possible explanation is obtained by examining the reduced frequency variation as the flow rate through the machine is reduced. The reduced frequency is the ratio of the time it takes a fluid particle to convect through the impeller channel to the time scale of the imposed unsteadiness. The time scale of the unsteadiness because of the downstream vane row potential field remains constant for a fixed rotational speed. However, because the convection time of the fluid particle increases as the flow rate is reduced, the reduced frequency value increases. Hence, unsteady interactions between the adjacent impeller blades may be becoming of increased significance at the lower flow rates even though the forcing-function amplitude is reduced. In addition, the maximum unsteady loading occurs over the central portion of the impeller blade for both radial spacings, and not near the exit as might be expected because this is where the forcing-function amplitude is largest. Also noted is that the measured unsteady loading distributions appear to be approaching zero near the trailing edge for all three operating points, indicating that the Kutta condition is satisfied. This is somewhat surprising considering the impeller blades have round, rather than sharp trailing edges.

Because of the rapid decay rate of the forcing function, a small increase in the radial spacing between the impeller and diffuser can result in a significant reduction in its amplitude and, hence, the resultant impeller blade unsteady aerodynamic response. This trend is present in both the individual surface pressure distributions and the resultant unsteady pressure difference across the blade. Figures 17 and 18 show that increasing the radial spacing results in roughly a 40% reduction in the maximum unsteady pressure difference across the blade for all three loading levels. However, even though the unsteady loading for the large spacing is considerably reduced over that at the small spacing, the loading still reaches quite large amplitudes at the lower flow rates.

Summary and Conclusions

A series of experiments was performed to investigate the unsteady aerodynamic response of a centrifugal compressor impeller because of its interaction with the potential field of the downstream radial-vaned diffuser. These experiments were performed over a range of flow rates for two different impeller–diffuser radial spacings. The forcing function to the impeller, i.e., the spatially nonuniform static pressure field at the diffuser inlet, and the resultant unsteady impeller blade surface pressure distributions were measured at each operating point.

Very near the vane leading-edge plane, multiple spatial harmonics were required to describe the forcing function. However, the spectrum of the impeller-blade response to each harmonic of this forcing function revealed a dominant vane-pass frequency. Thus, the higher harmonic components associated with this potential flow-generated forcing-function decay very rapidly across the vaneless space and do not contribute to the unsteady impeller-blade loading. Increasing the radial spacing between the impeller and diffuser significantly reduced both the amplitude of the forcing function and resulting unsteady aerodynamic loading on the impeller blades. Also, the maximum unsteady pressure difference across the impeller blade

occurred near midchord, and not near the exit where the diffuser vane-generated forcing function was largest.

Acknowledgment

This research was sponsored by the GUIde Consortium on Bladed Disk Forced Response.

References

[1]Inoue, M., and Cumpsty, N. A., "Experimental Study of Centrifugal Impeller Discharge Flow in Vaneless and Vaned Diffusers," *Journal of Engineering for Gas Turbines and Power*, Vol. 106, April 1984, pp. 455–467.

[2]Arndt, N., Acosta, A. J., Brennen, C. E., and Caughey, T. K., "Rotor-Stator Interaction in a Diffuser Pump," American Society of Mechanical Engineers, Paper 88-GT-55, June 1988.

[3]Arndt, N., Acosta, A. J., Brennen, C. E., and Caughey, T. K., "Experimental Investigation of Rotor-Stator Interaction in a Centrifugal Pump with Several Vaned Diffusers," *Journal of Turbomachinery*, Vol. 112, No. 1, 1990, pp. 98–108.

[4]Fisher, E. H., and Inoue, M., "A Study of Diffuser/Rotor Interaction in a Centrifugal Compressor," *Journal of Mechanical Engineering Science*, Vol. 23, No. 3, 1981, pp. 149–156.

[5]Bryan, W. B., and Fleeter, S., "Flow Induced Forced Response of an Incompressible Radial Cascade Including Profile and Incidence Effects," AIAA Paper 90-2352, July 1990.

[6]Whitehead, D. S., "Classical Two-Dimensional Methods," *AGARD Manual on Aeroelasticity in Axial-Flow Turbomachines, Unsteady Turbomachinery Aerodynamics*, Vol. 1, edited by M. F. Platzer and F. O. Carta, AGARD-AG-298, March 1987, Chap. III.

[7]Caruthers, J. E., and Kurosaka, M., "Flow Induced Vibration of Diffuser Excited Radial Compressors," NASA NAG 3-86, Sept. 1982.

[8]Schmidt, D. P., and Okiishi, T. H., "Multistage Axial-Flow Turbomachine Wake Production, Transport, and Interaction," *AIAA Journal*, Vol. 15, No. 8, 1977, pp. 1138–1145.

[9]Bryan, W. B., "An Investigation of Unsteady Impeller-Diffuser Interactions in a Centrifugal Compressor," Ph.D. Dissertation, Purdue Univ., West Lafayette, IN, Aug. 1991.